

# Lifetime Maximization for UAV-Enabled IoT Networks with Cognitive NOMA Transmissions

## Abstract

This paper investigates spectrum sharing communications in unmanned aerial vehicle (UAV) enabled internet of things (IoT) networks, where secondary/cognitive IoT devices simultaneously upload their data to the UAV following a non-orthogonal multiple access (NOMA) protocol in the pre-allocated spectrum to the primary network. We aim to maximize the minimum lifetime of IoT devices by jointly optimizing the UAV location, decoding order, and transmit power subject to probabilistic interference-power constraints at the primary base station (BS) while considering the imperfect channel state information (CSI). To solve the formulated non-convex mixed-integer programming problem, we first jointly optimize the UAV location and transmit power for given decoding order and obtain the globally optimal solution with the assistance of Lagrange duality. Then, by exhaustively searching all possible decoding orders, we obtain the global optimum to the formulated problem, which is applicable to relatively small-scale scenarios. For large-scale scenarios, we propose a low-complexity sub-optimal algorithm by transforming the original problem into a more tractable equivalent form and applying the successive convex approximation (SCA) technique and penalty function method. Numerical results demonstrate that the proposed design significantly outperforms the benchmark schemes.

## Index Terms

UAV communications, IoT, NOMA, cognitive radio, location optimization, power control.

## I. INTRODUCTION

Internet of Things (IoT) has been widely used in various applications, including smart home, soil monitoring, health-care, and manufacturing [1], [2]. Billions of intelligent devices capable of processing and sensing are anticipated to connect to the data center, which imposes critical

Na Tang is the first author. She is with the Science and Technology on Microsystem Laboratory, Shanghai Institute of Microsystem and Information Technology, Chinese Academy of Sciences, Shanghai 200050, China, and also with the University of Chinese Academy of Sciences, Beijing 100049, China.

challenges to spectrum resources. Due to size and cost constraints, many IoT devices carry drastically limited battery capacity and the lifetime of non-rechargeable devices is severely restricted. Once the battery of a device runs out, it is unable to support stable and reliable communications and even renders the network useless. Therefore, it is of utmost importance to efficiently utilize spectrum and battery resources to prolong the lifetime of IoT networks.

Cognitive radio (CR) technology has emerged as a prominent solution to spectrum scarcity issues. The basic idea of CR is to allow secondary users to use the licensed band of primary networks under interference constraints at primary users, thereby enhancing the spectrum utilization [3], [4]. However, CR cannot satisfy the demands of simultaneous transmission among massive devices, which arises as one of the biggest hurdles for IoT networks.

Non-orthogonal multiple access (NOMA) is proposed as an effective method to improve network access capabilities. A main principle of NOMA is to achieve time/frequency spectrum sharing and power domain multiplexing among multiple devices with the aid of superposition coding (SC) at the transmitter and successive interference cancellation (SIC) at the receiver. In this way, NOMA provides several advantages over orthogonal multiple access (OMA), such as high spectral efficiency, massive connectivity support, and low transmission latency [5], [6].

Unmanned aerial vehicles (UAVs) have been proposed as powerful aerial base stations (BSs) to serve ground users from the sky. With fully controllable mobility, employing UAVs to collect data from IoT devices can significantly shorten the communication distance and provide better channel quality. Compared with the terrestrial BS, UAVs have a much higher probability to connect IoT devices through line-of-sight (LoS) links, thus providing more reliable and energy-efficient wireless transmission. Thanks to these advantages, UAVs are perfectly matched with IoT networks, especially for devices with limited energy or installed in inaccessible areas. Therefore, the integration of CR, NOMA, and UAV can potentially enhance the efficiency of the spectrum and battery resources in IoT networks. This motivates us to investigate the cognitive NOMA transmission in UAV-enabled IoT networks.

#### *A. Related Work*

UAV-assisted communications have been widely investigated in the literature, in which UAVs are mainly employed as BSs [7]–[9] or relays [10], [11]. For instance, a UAV-enabled orthogonal frequency division multiple access (OFDMA) network is investigated in [7] to maximize the throughput by optimizing the UAV trajectory and resource allocation. Time-division multiple

access (TDMA) like wake-up scheduling scheme is proposed in [8] with the goal of minimizing the maximum energy consumption of sensors. For a UAV-enabled full-duplex relaying system, the work in [10] studies the joint design of bandwidth, power allocation, and the UAV trajectory to maximize the number of served IoT devices.

Extensive efforts have been devoted to studying the application of CR in UAV communications. There has been a proliferation of researches on employing the UAV to assist CR networks [12]–[14]. Specifically, the work in [12] uses the UAV as a relay to cooperate the communication of secondary users in energy-harvesting-based cognitive networks, while the work in [14] deploys the UAV as a friendly jammer to interfere with eavesdroppers. Moreover, there has been an increasing interest in cognitive UAV-enabled communications [15]–[17]. In [15], the UAV location/trajectory and transmit power are jointly optimized to maximize the SR's rates for quasi-stationary and mobile UAV scenarios, respectively. Ultra-reliable and low-latency communications are investigated in [17] to maximize the minimum finite block-length rate by optimizing the UAV altitude and power allocation.

Exploiting the attractive features of NOMA to further unlock the full potential of UAV communications has attracted great attention. Recent studies have investigated various objectives that include rate [18]–[22], UAV transmit power [22], [23], energy efficiency [24], number of served users [25], as well as secure transmission [26]–[28]. Among them, a data collection protocol is proposed in [18] to maximize the sum rate of a wireless sensor network by jointly optimizing the UAV placement, sensor grouping, and power control. The backhaul connectivity of the UAV-BS is considered in [23], where location and resource allocation are jointly optimized to minimize the UAV transmit power. [22] studies the joint optimization problem of location, decoding order, and power allocation with two goals of minimizing the UAV transmit power and maximizing the achievable rate of a user. Reference [24] investigates the joint resource allocation and UAV trajectory optimization for maximizing the total energy efficiency with the quality of service (QoS) requirement. To maximize the number of users with satisfied QoS, the work in [25] studies the UAV location design, admission control, and power allocation for NOMA transmission. In [27], two schemes are proposed to improve the security of NOMA-UAV networks via power allocation and beamforming optimization, respectively. In [26], the secrecy sum-rate maximization problem is studied for downlink transmission in a UAV-enabled cognitive NOMA network. However, these works largely ignore the lifetime performance in NOMA-based UAV communications.

There exist quite a few works focusing on lifetime maximization in UAV-enabled communication systems. The work in [29] optimizes user association, power, bandwidth allocation, and UAV deployment for maximizing the minimum lifetime in a multi-UAV enabled frequency division multiplexing access (FDMA) system. However, the results for FDMA systems cannot be directly applied to NOMA systems, due to different resource allocation mechanisms. For an ocean monitoring network with NOMA based device-to-UAV transmission, the authors in [30] study the multiple access, resource allocation, and UAV deployment issues to maximize network lifetime. However, in their model, the UAV location is first determined by sensors' positions and thus the decoding order is fixed based on channel gains of devices, which is strictly sub-optimal. Up to now, the joint optimization of UAV location, transmit power, and decoding order for improving the lifetime performance of NOMA networks has not been fully studied.

### *B. Contributions and Organization*

In this paper, we investigate the cognitive NOMA transmission in UAV-enabled IoT networks, where secondary IoT devices transmit data to the UAV with NOMA by accessing the spectrum allocated to the primary BS. Our goal is to maximize the minimum lifetime of IoT devices by jointly optimizing the UAV location, transmit power, and decoding order subject to the QoS requirement and probability interference constraints based on the imperfect channel state information (CSI) between IoT devices and BS. The main contributions of this paper can be summarized as follows.

- To the authors' best knowledge, this is the first work to study the lifetime maximization problem for cognitive NOMA transmission in UAV-enabled IoT networks.
- Although the formulated problem is non-convex mixed-integer and challenging to tackle, we solve it optimally by developing the Lagrange-duality-based algorithm. Specifically, for any given decoding permutation order, the optimal power and location are obtained in semi-closed forms. Then the problem resorts to enumerating all the possible decoding orders and determining the best performer that yields the highest lifetime. Note that the Lagrange-duality-based algorithm is applicable for small-scale scenarios in practice and can also serve as a benchmark for evaluating other algorithms.
- Furthermore, we also propose a low-complexity iterative algorithm, which can obtain a sub-optimal solution for large-scale scenarios. Specifically, by introducing binary variables to replace the complicated permutation variables, we construct an equivalent but more tractable

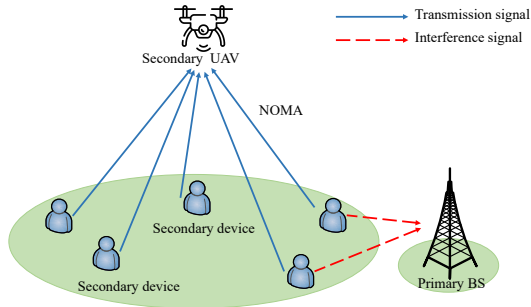


Fig. 1. A UAV-enabled IoT network with cognitive NOMA transmission.

problem. Then we derive a closed-form solution of the optimal power, by decoupling the mutual relationship between each user in the non-convex QoS constraints. Finally, the SCA technique and penalty function method are applied to approximate the location and decoding order problem into a series of convex problems.

- Numerical results demonstrate that the proposed joint optimization of UAV location, transmit power, and decoding order significantly outperforms the benchmark schemes. Besides, compared with the Lagrange-duality-based algorithm that achieves the optimal lifetime, the SCA-based iterative algorithm shows a slight performance degradation, which demonstrates that the SCA-based iterative algorithm is sub-optimal.

It is worth mentioning that different from previous works that only adopt binary variables [26], [31], [32] or permutation variables [22], [25], [33]–[35] to formulate the decoding order in NOMA transmission, our work unifies these two common decoding order formulations for the first time by proving the equivalence between the original problem and the newly constructed problem.

The rest of this paper is organized as follows. Section II introduces the system model and problem formulation for the cognitive NOMA transmission in UAV-enabled IoT networks. Section IV and Section III propose optimal and sub-optimal solutions to the formulated problem, respectively. In Section V, numerical results are presented to validate the effectiveness of the proposed joint design. Finally, we conclude the paper in Section VI.

*Notations:* In this paper, we use italic letters to denote scalars and bold lowercase letters to denote vectors.  $\mathbb{R}^{M \times 1}$  is the space of  $M$ -dimensional real-valued vectors. For a scalar  $x$ ,  $|x|$  is the absolute value. For a vector  $\mathbf{y}$ ,  $\|\mathbf{y}\|$  is the Euclidean norm, and  $\mathbf{y}^T$  denotes the transpose.

## II. SYSTEM MODEL AND PROBLEM FORMULATION

### A. System Model

As shown in Fig. 1, we consider a spectrum sharing scenario for a UAV-enabled IoT network, where  $K$  secondary IoT devices upload data to the UAV with NOMA over the licensed spectrum resource of the primary BS. Let  $\mathcal{K} = \{1, 2, \dots, K\}$  denote the set of ground IoT devices. Without loss of generality, we adopt a three-dimensional (3D) Cartesian coordinate system such that the horizontal coordinate of ground IoT device  $k$  is denoted as  $\mathbf{w}_k \in \mathbb{R}^{2 \times 1}$ ,  $k \in \mathcal{K}$ . Furthermore, we assume that the UAV is deployed at a constant altitude  $H$  with horizontal coordinate  $\mathbf{q} \in \mathbb{R}^{2 \times 1}$ . In this paper, we consider offline optimization by assuming that the UAV can get the specific location information of IoT devices in advance.

As commonly adopted in prior works on UAV communications [36], we assume that the ground-to-air communication channels are dominated by the LoS link. Therefore, the UAV can easily obtain CSI of devices based on location information [9]. In addition, we assume that the Doppler effect due to UAV mobility can be fully compensated. Following the free-space path loss model, the channel power gain from device  $k$  to the UAV can be expressed as

$$h_k = \rho_0 d_k^{-2} = \frac{\rho_0}{\|\mathbf{q} - \mathbf{w}_k\|^2 + H^2}, \quad (1)$$

where  $\rho_0$  denotes the channel power gain at the reference distance  $d_0 = 1$  m.

In uplink NOMA transmission, the UAV receives a superimposed signal of all devices and performs SIC to decode each signal. The device's signal with the highest channel gain (referred to as the strongest signal) is first decoded and then is subtracted from the aggregate signal. The same procedure is followed by the next strongest signal [37]. Consequently, the device with the highest channel gain (referred to as the strongest device) experiences interference from all devices, and the device with the lowest channel gain (referred to as the weakest device) effectively experiences interference-free transmission. For ease of exposition, denote the SIC decoding order at the UAV as  $\pi = \{\pi(1), \pi(2), \dots, \pi(K)\}$ , where  $\pi(m) = k$  means that the signal of device  $k$  is the  $m$ -th one to be decoded. As a result, the above constraints can be equivalently modeled as

$$\{\pi(1), \pi(2), \dots, \pi(K)\} \in \Psi, \quad (2)$$

$$h_{\pi(1)} \geq \dots \geq h_{\pi(K)}, \quad (3)$$

where  $\Psi$  denotes the set of all the  $K!$  possible permutations from 1 to  $K$ . Moreover, the signal from device  $\pi(n)$  with  $n > m$  is treated as interference when decoding the signal from device  $\pi(m)$ . Thus, the signal-to-interference-plus-noise ratio (SINR) of device  $\pi(m)$  is expressed as

$$\gamma_{\pi(m)} = \frac{p_{\pi(m)} h_{\pi(m)}}{\sum_{n=m+1}^K p_{\pi(n)} h_{\pi(n)} + \sigma^2}, \quad (4)$$

where  $p_{\pi(m)}$  denotes the transmit power of device  $\pi(m)$  and  $\sigma^2$  is the variance of Gaussian noise. Define the device lifetime as the uplink transmission time before its battery energy is drained. Then the lifetime of device  $\pi(m)$ , denoted by  $\tau_{\pi(m)}$  in second (s), can be expressed as

$$\tau_{\pi(m)} = \frac{E_{\pi(m)}}{p_{\pi(m)} + P_c}, \quad (5)$$

where  $E_{\pi(m)}$  denotes the battery energy of device  $\pi(m)$  and  $P_c$  denotes the circuit power consumption.

We assume a flat-fading channel between IoT device  $k$  and the primary BS, where the channel coefficient is denoted as  $c_{p,k}$ , which is an independent and identically distributed (i.i.d) zero mean circularly symmetric complex Gaussian (ZMCSCG) random variable, i.e.,  $CN(0, 1)$ . We further assume that IoT devices only have imperfect CSI of  $c_{p,k}$  and carry out minimum mean square error (MMSE) estimation of  $c_{p,k}$ , which is written as  $c_{p,k} = \check{c}_{p,k} + \Delta c_{p,k}$ , with  $\check{c}_{p,k}$  and  $\Delta c_{p,k}$  denoting the MMSE estimation of  $c_{p,k}$  and corresponding estimation error, respectively. According to the property of MMSE estimation,  $\check{c}_{p,k}$  and  $\Delta c_{p,k}$  are uncorrelated and are ZMCSCG distributed with variance  $1 - \sigma_e^2$  and  $\sigma_e^2$ , respectively. The channel power gains are denoted as  $z_k$ ,  $\tilde{z}_k$  and  $\Delta z_k$  with  $z = |c|^2$ , and the corresponding probability density functions can be, respectively, expressed as

$$f(z_k) = \exp(-z_k), f(\tilde{z}_{p,k}) = \frac{1}{1 - \varepsilon_p^2} \exp\left(-\frac{\tilde{z}_{p,k}}{1 - \varepsilon_p^2}\right), f(\Delta z_{p,k}) = \frac{1}{\varepsilon_p^2} \exp\left(-\frac{\Delta z_{p,k}}{\varepsilon_p^2}\right). \quad (6)$$

Since IoT devices only obtain the imperfect estimation of  $\tilde{z}_{p,k}$ , it cannot strictly ensure that the interference peak power at primary BS is below the threshold  $I_{th}$ . Assume that the transmission of IoT devices is allowed to exceed the peak threshold with a certain probability  $\varrho$ , i.e.,

$$\Pr\{p_{\pi(m)} z_{\pi(m)} \geq I_{th}\} \leq \varrho, \forall m. \quad (7)$$

## B. Problem Formulation

Let  $\mathbf{p} = \{p_{\pi(m)}, m \in \mathcal{K}\}$ . By taking into account the QoS requirement and probability interference constraints, our objective is to maximize the minimum lifetime of IoT devices via

jointly optimizing the UAV location  $\mathbf{q}$ , transmit power  $\mathbf{p}$ , and decoding order  $\boldsymbol{\pi}$ . Mathematically, the optimization problem can be formulated as

$$\max_{\eta, \mathbf{q}, \mathbf{p}, \boldsymbol{\pi}} \quad \eta \quad (8a)$$

$$\text{s.t.} \quad \frac{E_{\pi(m)}}{p_{\pi(m)} + P_c} \geq \eta, \forall m, \quad (8b)$$

$$0 \leq p_{\pi(m)} \leq P_{\max}, \forall m, \quad (8c)$$

$$\log_2(1 + \gamma_{\pi(m)}) \geq r^*, \forall m, \quad (8d)$$

$$(2), (3), (7), \quad (8e)$$

where  $P_{\max}$  is the maximum transmit power of devices and  $r^*$  denotes the QoS requirement for all devices. Due to the existence of non-convex constraints (2), (3), (7), (8b), and (8d) as well as the permutation variable  $\boldsymbol{\pi}$  that lacks closed-form expression, problem (8) is a mixed-integer non-convex optimization problem, which is generally hard to solve.

To facilitate the processing of problem (8), we transform it into a more tractable form by exploiting the hidden convexity of the non-convex constraints in the following. First, based on the results in [38], the probability interference constraints (7) can be guaranteed by a sufficient instantaneous power constraint, which is expressed as

$$p_{\pi(m)} \leq \frac{I_{th}}{z_{\pi(m)} - \varepsilon_p^2 \ln \varrho}. \quad (9)$$

From (1), constraint (3) can be equivalently rewritten as

$$d_{\pi(1)} \leq d_{\pi(2)} \leq \cdots \leq d_{\pi(K)}. \quad (10)$$

Moreover, we introduce the slack variable  $\zeta = \frac{1}{\eta}$ , by which problem (8) can be transformed into

$$\min_{\zeta, \mathbf{q}, \mathbf{p}, \boldsymbol{\pi}} \quad \zeta \quad (11a)$$

$$\text{s.t.} \quad p_{\pi(m)} + P_c \leq \zeta E_{\pi(m)}, \forall m, \quad (11b)$$

$$0 \leq p_{\pi(m)} \leq \tilde{P}_{\pi(m)}, \forall m, \quad (11c)$$

$$(8d), (10), \quad (11d)$$

where  $\tilde{P}_{\pi(m)} \triangleq \min\{P_{\max}, \frac{I_{th}}{z_{\pi(m)} - \varepsilon_p^2 \ln \varrho}\}$  that will be referred to as the allowable power in the following content. Note that the non-convex constraints (8b) have been converted into linear

constraints (11b), which greatly reduces the computational complexity. Problem (11) is still mixed-integer non-convex due to non-convex constraints (8d) and (10) as well as the permutation variable  $\pi$ . In general, it is quite challenging to solve such a problem optimally. In the next two sections, we propose an optimal algorithm as well as a low-complexity sub-optimal algorithm for solving problem (11) by applying the Lagrange duality, SCA technique and penalty method, respectively.

### III. GLOBAL OPTIMIZATION SOLUTION

In this section, we provide a globally optimal solution of problem (11) by proposing the Lagrange-duality-based algorithm. Specifically, for given decoding order  $\pi$ , we first derive a closed-form expression of the optimal power  $\mathbf{p}$  and thereby reduce the joint design to the location  $\mathbf{q}$  optimization problem that is convex. Then, the optimal  $\mathbf{q}$  is obtained in a semi-closed form. Finally, by searching all possible decoding orders and picking out the best performer, we obtain the global optimum to problem (11).

#### A. Joint Location and Transmit Power Optimization

For any given decoding order  $\pi$ , the UAV location and transmit power  $\{\mathbf{q}, \mathbf{p}\}$  can be optimized by solving the following problem.

$$\min_{\zeta, \mathbf{q}, \mathbf{p}} \zeta \quad (12a)$$

$$\text{s.t. } p_{\pi(m)} + P_c \leq \zeta E_{\pi(m)}, \forall m, \quad (12b)$$

$$0 \leq p_{\pi(m)} \leq \tilde{P}_{\pi(m)}, \forall m, \quad (12c)$$

$$(8d), (10). \quad (12d)$$

Problem (29) is a non-convex optimization problem due to non-convex constraints (8d) and (10). By exploiting problem structure and the hidden convexity, we propose an efficient algorithm based on Lagrange duality to determine the optimal  $\{\mathbf{q}, \mathbf{p}\}$ . Specifically, note that constraints (10) can be equivalently rewritten as

$$\|\mathbf{q} - \mathbf{w}_{\pi(1)}\|^2 \leq \|\mathbf{q} - \mathbf{w}_{\pi(2)}\|^2 \leq \dots \leq \|\mathbf{q} - \mathbf{w}_{\pi(K)}\|^2. \quad (13)$$

However, due to  $\|\mathbf{q} - \mathbf{w}_{\pi(m)}\|^2 - \|\mathbf{q} - \mathbf{w}_{\pi(m+1)}\|^2 = 2(\mathbf{w}_{\pi(m+1)} - \mathbf{w}_{\pi(m)})^T \mathbf{q} - \|\mathbf{w}_{\pi(m+1)}\|^2 + \|\mathbf{w}_{\pi(m)}\|^2$ , constraints (13) are further transformed into

$$2(\mathbf{w}_{\pi(m+1)} - \mathbf{w}_{\pi(m)})^T \mathbf{q} \leq \|\mathbf{w}_{\pi(m+1)}\|^2 - \|\mathbf{w}_{\pi(m)}\|^2, \forall m = 1, \dots, K-1, \quad (14)$$

which are linear with respect to  $\mathbf{q}$ . Moreover, constraints (8d) can be reformulated as

$$p_{\pi(m)}h_{\pi(m)} \geq (2^{r^*} - 1) \left( \sum_{n=m+1}^K p_{\pi(n)}h_{\pi(n)} + \sigma^2 \right), \forall m. \quad (15)$$

Thus, problem (12) is equivalent to

$$\min_{\zeta, \mathbf{q}, \mathbf{p}} \quad \zeta \quad (16a)$$

$$\text{s.t.} \quad p_{\pi(m)} + P_c \leq \zeta E_{\pi(m)}, \forall m, \quad (16b)$$

$$(12c), (14), (15). \quad (16c)$$

Combining (16a) and (16b), it can be verified that we have  $\zeta(\mathbf{p}) = \max_m \left\{ \frac{p_{\pi(m)} + P_c}{E_{\pi(m)}} \right\}$  at the optimal solution, since otherwise, we may further decrease  $\zeta$  without violating constraints (16b). This indicates that  $\zeta(\mathbf{p})$  is monotonic increasing with respect to  $p_{\pi(m)}$ . Thus, the optimal power  $p_{\pi(m)}^*$  should always be the lower bound, which can be obtained from constraints (15), i.e.,

$$p_{\pi(m)}^* = \frac{(2^{r^*} - 1) \left( \sum_{n=m+1}^K p_{\pi(n)}^* h_{\pi(n)} + \sigma^2 \right)}{h_{\pi(m)}}, \forall m. \quad (17)$$

Note that the power allocations in (17) are mutually coupled with that of each device. Hence, in the following lemma, we will decouple this relationship, and give a closed-form of  $p_{\pi(m)}^*$ .

*Lemma 1:* Let  $c_m \triangleq \frac{(2^{r^*} - 1)\sigma^2}{\rho_0} 2^{(K-m)r^*}$  and then the closed-form solution of  $p_{\pi(m)}^*$  is given by

$$p_{\pi(m)}^* = c_m (H^2 + \|\mathbf{q} - w_{\pi(m)}\|^2), \forall m. \quad (18)$$

*Proof 1:* See Appendix A.

With Lemma 1, problem (16) reduces to the following problem for optimizing  $\mathbf{q}$  only, i.e.,

$$\min_{\zeta, \mathbf{q}} \quad \zeta \quad (19a)$$

$$\text{s.t.} \quad P_c + c_m (H^2 + \|\mathbf{q} - w_{\pi(m)}\|^2) \leq \zeta E_{\pi(m)}, \forall m, \quad (19b)$$

$$H^2 + \|\mathbf{q} - w_{\pi(m)}\|^2 \leq \bar{P}_{\pi(m)}, \forall m, \quad (19c)$$

$$(14), \quad (19d)$$

where  $\bar{P}_{\pi(m)} \triangleq \frac{1}{c_m} \min\{P_{\max}, \frac{I_{th}}{z_{\pi(m)} - \varepsilon_p^2 \ln \varrho}\}$ . Problem (19) is convex and satisfying Slater's constraint qualification. As a result, the optimal solution of problem (19) can be obtained by solving its dual problem. Denote  $\boldsymbol{\lambda}$ ,  $\boldsymbol{\mu}$ , and  $\mathbf{v}$  as the non-negative Lagrange multipliers for constraints

(19b), (19c), and (14), respectively. The Lagrange function of problem (19) can be derived in (23) at the top of the next page. Accordingly, the dual function is given by

$$f(\boldsymbol{\lambda}, \boldsymbol{\mu}, \mathbf{v}) = \min_{\zeta, \mathbf{q}} \mathcal{L}(\zeta, \mathbf{q}, \boldsymbol{\lambda}, \boldsymbol{\mu}, \mathbf{v}), \quad (20)$$

for which the following lemma holds.

*Lemma 2:* To make  $f(\boldsymbol{\lambda}, \boldsymbol{\mu}, \mathbf{v})$  bounded from the above, i.e.,  $f(\boldsymbol{\lambda}, \boldsymbol{\mu}, \mathbf{v}) < +\infty$ , it holds that  $\sum_{m=1}^K \lambda_m E_{\pi(m)} = 1$ .

*Proof 2:* If  $\sum_{m=1}^K \lambda_m E_{\pi(m)} > 1$  or  $\sum_{m=1}^K \lambda_m E_{\pi(m)} < 1$ , then we have  $f(\boldsymbol{\lambda}, \boldsymbol{\mu}, \mathbf{v}) \rightarrow +\infty$  by setting  $\zeta \rightarrow +\infty$  or  $\zeta \rightarrow -\infty$ . This contradicts that the dual function is bound, which completes the proof.  $\blacksquare$

Problem (20) is convex such that the optimal solution can be obtained by applying Karush-KuhnTucker (KKT) conditions, i.e.,

$$\mathbf{q}^* = \frac{\sum_{m=1}^K (c_m \lambda_m + \mu_m) \mathbf{w}_{\pi(m)} + \sum_{m=1}^{K-1} v_m (\mathbf{w}_{\pi(m)} - \mathbf{w}_{\pi(m+1)})}{\sum_{m=1}^K (c_m \lambda_m + \mu_m)}. \quad (21)$$

After obtaining  $\mathbf{q}^*$  for any given  $\{\boldsymbol{\lambda}, \boldsymbol{\mu}, \mathbf{v}\}$ , the dual problem of (19) is given by

$$\max_{\boldsymbol{\lambda}, \boldsymbol{\mu}, \mathbf{v}} f(\boldsymbol{\lambda}, \boldsymbol{\mu}, \mathbf{v}) \quad (22a)$$

$$\text{s.t.} \quad \sum_{m=1}^K \lambda_m E_{\pi(m)} = 1, \quad (22b)$$

$$\boldsymbol{\lambda} \succeq 0, \boldsymbol{\mu} \succeq 0, \mathbf{v} \succeq 0. \quad (22c)$$

Problem (22) can be solved via a subgradient-based method such as the ellipsoid method. Specifically, the subgradient of the objective function is denoted by  $\boldsymbol{\eta}_0 = [\Delta \boldsymbol{\lambda}, \Delta \boldsymbol{\mu}, \Delta \mathbf{v}]^T$  with  $\Delta \lambda_m = -c_m \|\mathbf{q}^* - \mathbf{w}_{\pi(m)}\|^2 - (c_m H^2 + P_c)$ ,  $\Delta \mu_m = -\|\mathbf{q}^* - \mathbf{w}_{\pi(m)}\|^2 - (H^2 - \bar{P}_{\pi(m)})$ , and  $\Delta v_m = -2(\mathbf{w}_{\pi(m+1)} - \mathbf{w}_{\pi(m)})^T \mathbf{q}^* + \|\mathbf{w}_{\pi(m+1)}\|^2 - \|\mathbf{w}_{\pi(m)}\|^2, \forall m$ . Moreover, the equality constraint (22b) is equivalent to two inequality constraints, i.e.,  $\sum_{m=1}^K \lambda_m E_{\pi(m)} \geq 1$  and  $\sum_{m=1}^K \lambda_m E_{\pi(m)} \leq 1$ , whose subgradients are denoted by  $\boldsymbol{\eta}_1 = [\Delta \boldsymbol{\lambda}, \Delta \boldsymbol{\mu}, \Delta \mathbf{v}]^T$  with  $\Delta \lambda_m = -E_{\pi(m)}, \Delta \mu_m = 0, \Delta v_k = 0, \forall k$  and  $\boldsymbol{\eta}_2 = [\Delta \boldsymbol{\lambda}, \Delta \boldsymbol{\mu}, \Delta \mathbf{v}]^T$  with  $\Delta \lambda_m = E_{\pi(m)}, \Delta \mu_m = 0, \Delta v_m = 0, \forall m$ , respectively. After obtaining the optimal location  $\mathbf{q}^*$ , the corresponding optimal transmit power  $\mathbf{p}^*$  can be directly calculated using (18) and objective value  $\zeta^*$  can be obtained as  $\zeta^* = \max_m \left\{ \frac{p_{\pi(m)}^* + P_c}{E_{\pi(m)}} \right\}$ . The details of the procedures for solving problem (12) are summarized in Algorithm 1. The complexity of Algorithm 1 is  $O(K^4)$ .

---


$$\begin{aligned}
\mathcal{L}(\zeta, \mathbf{q}, \boldsymbol{\lambda}, \boldsymbol{\mu}) &= (1 - \sum_{m=1}^K \lambda_m E_{\pi(m)}) \zeta + \sum_{m=1}^K (\lambda_m c_m + \mu_m) \|\mathbf{q} - \mathbf{w}_{\pi(m)}\|^2 + \sum_{m=1}^K (\lambda_m (c_m H^2 + P_c) + \mu_m (H^2 - \bar{P}_{\pi(m)})) \\
&+ 2 \sum_{m=1}^{K-1} v_m (\mathbf{w}_{\pi(m+1)} - \mathbf{w}_{\pi(m)})^T \mathbf{q} + \sum_{m=1}^{K-1} v_m (\|\mathbf{w}_{\pi(m)}\|^2 - \|\mathbf{w}_{\pi(m+1)}\|^2). \tag{23}
\end{aligned}$$


---

---

**Algorithm 1** Joint Location and Transmit Power Algorithm for Solving Problem (12)

---

- 1: Initialize  $\boldsymbol{\lambda}, \boldsymbol{\mu}, \mathbf{v}$  and the ellipsoid.
  - 2: **repeat**
  - 3:   Obtain  $\mathbf{q}^*$  by (21).
  - 4:   Compute the subgradients of objective function and constraint functions in problem (22).
  - 5:   Update  $\{\boldsymbol{\lambda}, \boldsymbol{\mu}, \mathbf{v}\}$  by using the constrained ellipsoid method.
  - 6: **until**  $\boldsymbol{\lambda}, \boldsymbol{\mu}, \mathbf{v}$  converge within a prescribed accuracy.
  - 7: Set  $\{\boldsymbol{\lambda}^*, \boldsymbol{\mu}^*, \mathbf{v}^*\} \leftarrow \{\boldsymbol{\lambda}, \boldsymbol{\mu}, \mathbf{v}\}$ .
  - 8: Obtain  $\mathbf{q}^*, \mathbf{p}^*$  and  $\zeta^*$  by using (21) and (18).
- 

---

**Algorithm 2** Globally Optimal: Proposed Lagrange-duality-based Algorithm for Solving Problem (11)

---

- 1: Set the number  $l = 0$ .
  - 2: Find  $K!$  decoding orders and represent them as the set  $\mathcal{P} = \{\mathcal{P}_1, \dots, \mathcal{P}_{K!}\}$ .
  - 3: **for**  $l = 1$  to  $K!$  **do**
  - 4:   Set  $\{\pi^l(1), \pi^l(2), \dots, \pi^l(K)\} \leftarrow \mathcal{P}_l$ .
  - 5:   Solve problem (12) by applying Algorithm 1 for given  $\pi^l$ , and denote the optimal solution as  $\{\zeta^l, \mathbf{q}^l, \mathbf{p}^l\}$ .
  - 6:   **if**  $\zeta^l \leq \zeta^*$  **then**
  - 7:     Set  $\{\zeta^*, \mathbf{q}^*, \mathbf{p}^*, \boldsymbol{\pi}^*\} \leftarrow \{\zeta^l, \mathbf{q}^l, \mathbf{p}^l, \boldsymbol{\pi}^l\}$ .
  - 8:   **end if**
  - 9: **end for**
  - 10: Obtain the optimal solution as  $\{\mathbf{q}^*, \mathbf{p}^*, \boldsymbol{\pi}^*\}$ .
-

### B. Decoding Order Optimization and Overall Algorithm

We will exhaustively search all the  $K!$  possible decoding orders while obtaining the globally optimal UAV location  $\mathbf{q}$  and transmit power  $\mathbf{p}$  via Algorithm 1 in each inner loop. The globally optimal value and solution of problem (11) are the maximum value determined by all possible decoding orders and the corresponding  $\{\mathbf{q}, \mathbf{p}, \boldsymbol{\pi}\}$ , respectively. The details of the procedures are summarized in Algorithm 2. The complexity of Algorithm 2 is  $O(K^4 K!)$ .

*Remark 1:* Although Algorithm 2 entails high complexity, it provides a practically feasible method to obtain the global optimal solution. Moreover, Algorithm 2 is feasible for relatively small-scale IoT networks and can also serve as a benchmark for evaluating other algorithms.

## IV. LOW-COMPLEXITY SUBOPTIMAL SOLUTION

The Lagrange-duality-based algorithm in the preceding section provides an optimal solution to problem (11). However, the computational complexity of the algorithm is relatively high. In this section, as an alternative, we propose a low-complexity iterative algorithm for solving problem (11), which yields a sub-optimal solution for large-scale IoT networks. Specifically, we first reformulate problem (11) into an equivalent but more tractable form by introducing binary variables to replace the permutation variables and showing their explicit relationship. Next, we derive a closed-form solution of the optimal power and then apply the SCA technique and penalty function method to obtain a sub-optimal solution.

### A. Equivalent Reformulation of Problem (11)

As shown in Section III, the main complexity of Algorithm 2 lies in the exhaustive search over  $K!$  possible solutions. To reduce the complexity, in this section, we first introduce auxiliary

variables  $\alpha = \{\alpha_{k,j}, k, j \in \mathcal{K}\}$  and the following problem.

$$\min_{\zeta, \mathbf{q}, \mathbf{p}, \alpha} \zeta \quad (24a)$$

$$\text{s.t. } p_k + P_c \leq \zeta E_k, \forall k, \quad (24b)$$

$$0 \leq p_k \leq \tilde{P}_k, \forall k, \quad (24c)$$

$$\log_2 \left( 1 + \frac{p_k h_k}{\sum_{j=1, j \neq k}^K \alpha_{k,j} p_j h_j + \sigma^2} \right) \geq r^*, \forall k, \quad (24d)$$

$$\alpha_{k,j} = \begin{cases} 0, & \text{if } d_k > d_j, \\ 1, & \text{if } d_k < d_j, \\ 0 \text{ or } 1, & \text{if } d_k = d_j, \end{cases} \quad \forall k \neq j, \quad (24e)$$

$$\alpha_{k,k} = 0, \forall k, \quad (24f)$$

$$\alpha_{k,j} + \alpha_{j,k} = 1, \forall k \neq j, \quad (24g)$$

$$\alpha_{k,j} + \alpha_{j,i} - 1 \leq \alpha_{k,i}, \forall k, j, i, \quad (24h)$$

where  $k, j, i \in \mathcal{K}$  denote the device indexes and are fixed.

*Remark 2:* In fact, the SIC procedure can be guaranteed by satisfying constraints (24e)-(24h), as elaborated below. First, let  $\alpha_{k,j} = 1$  denote that the signal of device  $k$  is decoded before that of device  $j$ ; otherwise,  $\alpha_{k,j} = 0$ . Then, the practical meanings of constraints (24e)-(24g) can refer to work [26]. Constraints (24h) ensure that when  $\alpha_{k,j} = 1$  and  $\alpha_{j,i} = 1$ , it must have  $\alpha_{k,i} = 1$ ; otherwise,  $\alpha_{k,i} \geq 0^1$ . This implies that if the signal of device  $k$  is decoded before that of device  $j$ , and the signal of device  $j$  is decoded before that of device  $i$ , then the signal of device  $k$  must be decoded before that of device  $i$ .

In the following, we first present the explicit relationship between  $\pi$  and  $\alpha$  and then prove that problems (11) and (24) share the same optimal value. To proceed, an important and useful transformation of constraint (24d) is given in the following proposition.

*Proposition 1:* If  $\alpha$  satisfies constraints (24d)-(24h), then constraints (24d) are equivalent to  $f(k) = K - \sum_{j=1}^K \alpha_{k,j}$  and

$$\log_2 \left( 1 + \frac{p_k h_k}{\sum_{f(j)=f(k)+1}^K p_j h_j + \sigma^2} \right) \geq r^*, \forall k. \quad (25)$$

<sup>1</sup>Such a relationship can also be written as  $\alpha_{k,j} \alpha_{j,i} \leq \alpha_{k,i}, \forall k, j, i$  [35]. However, the constraints in [35] are non-convex. By contrast, our proposed constraints (24h) are linear and easier to handle.

*Proof 3:* See Appendix B.

Then, we come to reveal how to obtain a feasible solution of problem (11)/(24) from the solution of problem (24)/(11) in the following propositions.

*Proposition 2:* For any feasible solution  $\{\boldsymbol{\alpha}, \mathbf{p}, \mathbf{q}\}$  of problem (24), we can construct  $\{\boldsymbol{\pi}', \mathbf{p}', \mathbf{q}\}$  with  $\mathbf{p}' = [p'_1, \dots, p'_K]^T$ , as a feasible solution of problem (11) by setting  $\pi' = f^{-1}$  and  $p'_{\pi'(m)} = p_{f^{-1}(m)}$ . Moreover, the objective value of problem (11) obtained at  $\{\boldsymbol{\pi}', \mathbf{p}', \mathbf{q}\}$  is the same as that of problem (24) obtained at  $\{\boldsymbol{\alpha}, \mathbf{p}, \mathbf{q}\}$ <sup>2</sup>.

*Proof 4:* See Appendix C.

*Proposition 3:* For any feasible solution  $\{\boldsymbol{\pi}, \mathbf{p}, \mathbf{q}\}$  of problem (11), we can construct  $\{\tilde{\boldsymbol{\alpha}}, \tilde{\mathbf{p}}, \mathbf{q}\}$  with  $\tilde{\boldsymbol{\alpha}} = \{\tilde{\alpha}_{k,j}, k, j \in \mathcal{K}\}$  and  $\tilde{\mathbf{p}} = [\tilde{p}_1, \dots, \tilde{p}_K]^T$  as a feasible solution of problem (24) by setting  $\tilde{p}_k = p_{\pi(m)}$  and

$$\tilde{\alpha}_{\pi(m), \pi(n)} = \begin{cases} 1, & \text{if } m < n, \\ 0, & \text{otherwise.} \end{cases} \quad (26)$$

Moreover, the objective value of problem (24) obtained at  $\{\tilde{\boldsymbol{\alpha}}, \tilde{\mathbf{p}}, \mathbf{q}\}$  is identical to that of problem (11) obtained at  $\{\boldsymbol{\pi}, \mathbf{p}, \mathbf{q}\}$ .

*Proof 5:* See Appendix D.

We are now ready to clarify the equivalence between problems (11) and (24).

*Proposition 4:* Problem (24) can achieve the same optimal value as problem (11).

*Proof 6:* Define  $L_1$  and  $L_2$  as the optimal value of problem (11) and problem (24), respectively. Based on Proposition 2 and 3, we have  $L_1 \leq L_2$  and  $L_1 \geq L_2$ , respectively. Thus,  $L_1 = L_2$ . ■

It should be noted that in the literature, both binary variables  $\alpha_{k,j}$  as well as permutation variables  $\boldsymbol{\pi}$  are adopted for decoding order formulations, such as [22], [25], [26], [31]–[35]. However, these two different problem formulations are used alternatively without any explicit relationship and thus have always been treated as two independent programs. Furthermore, only a sub-optimal solution of  $\boldsymbol{\alpha}$ -related programs can be obtained by relaxing the binary constraints and applying the SCA technique in general. It yet remains unknown whether these two problem formulations can achieve the same optimal performance. In this paper, we prove that they can be used interchangeably via Propositions 2-4 and thus unify these two problems for the first time in the literature.

<sup>2</sup>Furthermore, owing to the definition of  $\boldsymbol{\pi}$  and  $\pi = f^{-1}$  in Propositions 2, we have  $m = \pi^{-1}(k) = f(k)$ , which means that the signal from device  $k$  should be decoded at the  $f(k)$ -th (i.e.,  $K - \sum_{j=1}^K \alpha_{k,j}$ ).

### B. Closed-form Solution of Transmit Power

Based on proposition 4, we only need to focus on solving problem (24) with the non-convex constraints (24d)-(24e) and binary variables  $\alpha$ . In general, there is no standard method to solve such a problem optimally. In this subsection, we will derive an explicit analytical solution of  $p_k$  as a function of  $\alpha$  and  $\mathbf{q}$  based on (25), by which problem (24) can be greatly simplified.

By Proposition 1, problem (24) can be equivalently written as

$$\min_{\zeta, \mathbf{q}, \mathbf{p}, \boldsymbol{\alpha}, f} \zeta \quad (27a)$$

$$\text{s.t. } p_k \geq \frac{(2^{r^*} - 1) \left( \sum_{f(j)=f(k)+1}^K p_j h_j + \sigma^2 \right)}{h_k}, \forall k, \quad (27b)$$

$$f(k) = K - \sum_{j=1}^K \alpha_{k,j}, \forall k, \quad (27c)$$

$$(24b), (24c), (24e) - (24h). \quad (27d)$$

As we can see, the objective function  $\zeta(\mathbf{p}) = \max_k \{ \frac{p_k + P_c}{E_k} \}$  of problem (27) is increasing with  $p_k$ . Thus, the optimal  $\mathbf{p}^*$  should always be the lower bound, which can be obtained when constraints (27b) satisfy strict equality. To obtain  $\mathbf{p}^*$ , define  $p_{f(k)}^s = p_k$  and  $h_{f(k)}^s(\mathbf{w}_{f(k)}^s) = h_k(\mathbf{w}_k)$ . Then constraint (27b) can be rewritten as

$$p_{f(k)}^s \geq \frac{(2^{r^*} - 1)}{h_{f(k)}^s} \left( \sum_{f(j)=f(k)+1}^K p_{f(j)}^s h_{f(j)}^s + \sigma^2 \right).$$

By following the similar lines as previous proofs of Lemma 1, we can obtain the optimal  $p_{f(k)}^{s*} = c_{f(k)}(H^2 + \|\mathbf{q} - \mathbf{w}_{f(k)}^s\|^2)$ , where  $c_{f(k)} \triangleq \frac{(2^{r^*} - 1)\sigma^2}{\rho_0} 2^{(K-f(k))r^*}$ . This yields

$$p_k^* = c_{f(k)}(H^2 + \|\mathbf{q} - \mathbf{w}_k\|^2). \quad (28)$$

By adopting a similar approach in our previous work [26], the non-smooth constraints (24e) can be equivalently transformed into a smooth form as follows.

$$\sum_{k,j}^K (\alpha_{k,j} - \alpha_{k,j}^2) \leq 0, \quad (29a)$$

$$\sum_{k,j}^K g_{k,j}(\alpha_{k,j}, \mathbf{q}) \leq 0, \quad (29b)$$

$$0 \leq \alpha_{k,j} \leq 1, \forall k, j, \quad (29c)$$

where  $g_{k,j}(\alpha_{k,j}, \mathbf{q}) \triangleq \theta_{k,j}(2\alpha_{k,j} - 1) + |\theta_{k,j}|$  and  $\theta_{k,j} \triangleq 2(\mathbf{w}_j - \mathbf{w}_k)^T \mathbf{q} + \|\mathbf{w}_k\|^2 - \|\mathbf{w}_j\|^2$ . Note that  $\theta_{k,j}$  is linear with respect to  $\mathbf{q}$  and  $|\theta_{k,j}|$  is convex with respect to  $\mathbf{q}$  [26]. With (28) and (29), problem (27) reduces to

$$\min_{\zeta, \mathbf{q}, \boldsymbol{\alpha}, f} \zeta \quad (30a)$$

$$\text{s.t. } c_{f(k)} (H^2 + \|\mathbf{q} - \mathbf{w}_k\|^2) + P_c \leq \zeta E_k, \forall k, \quad (30b)$$

$$c_{f(k)} (H^2 + \|\mathbf{q} - \mathbf{w}_k\|^2) \leq \tilde{P}_k, \forall k, \quad (30c)$$

$$(24f) - (24h), (27c), (29). \quad (30d)$$

### C. SCA-Based Optimization

The main challenge of problem (30) lies in that  $f$  is involved as the index in constraints (30b) and (30c). A close observation of problem (30) shows that we can solve the following sub-problems alternately: sub-problem 1 optimizes  $f$  with given  $\boldsymbol{\alpha}$ , whose optimal solution can be obtained from constraints (27c), i.e.,

$$f^*(k) = K - \sum_{j=1}^K \alpha_{k,j}, \quad (31)$$

and subproblem 2 optimizes  $\{\mathbf{q}, \boldsymbol{\alpha}\}$  with given  $f$ , i.e.,

$$\min_{\zeta, \mathbf{q}, \boldsymbol{\alpha}} \zeta \quad (32a)$$

$$\text{s.t. } (24f) - (24h), (29), (30b), (30c). \quad (32b)$$

The remaining task is to solve problem (32) with non-convex constraints (29a) and (29b). With loss of generality, we can leverage the SCA technique to approximate the non-convex term to a convex form in each iteration and then iteratively solve a series of approximated convex problems. However, the SCA technique cannot be straightforwardly applied to constraints (29a) and (29b) since there may be some iterations where the approximated problem is infeasible due to (29c). To overcome this obstacle, we introduce slack variables  $\phi$  and  $\varphi$  and take into account the relaxed version of problem (32) as

$$\min_{\zeta, \mathbf{q}, \boldsymbol{\alpha}} \zeta + \rho_1 \phi + \rho_2 \varphi \quad (33a)$$

$$\text{s.t. } (24f) - (24h), (29c), (30b) - (30c), \quad (33b)$$

where  $\phi \triangleq \sum_{k,j}^K (\alpha_{k,j} - \alpha_{k,j}^2)$  and  $\varphi \triangleq \sum_{k,j}^K g_{k,j}(\alpha_{k,j}, \mathbf{q})$ , and  $\rho_1 > 0$  and  $\rho_2 > 0$  are penalty parameters. It is worth noting that it must have  $\phi \geq 0$  and  $\varphi \geq 0$  due to  $\alpha_{k,j} - \alpha_{k,j}^2 \geq 0$  and  $g_{k,j}(\alpha_{k,j}, \mathbf{q}) \geq 0$  within the feasible region of problem (33). Inspired by [25], it can be proved that problem (33) is equivalent to (32), when  $\rho_1 \geq \rho_1^*$  and  $\rho_2 \geq \rho_2^*$ , with  $\rho_1^*$  and  $\rho_2^*$  denoting the optimal Lagrange multiplier of constraints (29a) and (29b), respectively. In the following, we transform the non-convex constraints (29a) and (29b) into convex constraints by deriving the global lower bounds at a given point. Specifically, based on the fact that the first-order Taylor expansion of concave function is its global over-estimator, we have the following upper bound for  $\phi$  at any local point  $\{\bar{\alpha}_{k,j}\}$ , i.e.,

$$\phi \leq \sum_{k,j}^K (\alpha_{k,j}^2 + \bar{\alpha}_{k,j}^2 - 2\bar{\alpha}_{k,j}\alpha_{k,j}) \triangleq \bar{\phi}. \quad (34)$$

In addition, we can obtain the upper bound of  $\alpha_{k,j}\theta_{k,j}$  at any local point  $\{\bar{\mathbf{q}}, \bar{\alpha}_{k,j}\}$  as

$$\begin{aligned} 2\alpha_{k,j}\theta_{k,j} &= \frac{1}{2} [(\theta_{k,j} + \alpha_{k,j})^2 - (\theta_{k,j} - \alpha_{k,j})^2] \\ &\leq \frac{1}{2} [(\theta_{k,j} + \alpha_{k,j})^2 + (\bar{\theta}_{k,j} - \bar{\alpha}_{k,j})^2] - (\bar{\theta}_{k,j} - \bar{\alpha}_{k,j})(\theta_{k,j} - \alpha_{k,j}) \triangleq D_{k,j}, \end{aligned} \quad (35)$$

where  $\bar{\theta}_{k,j} \triangleq 2(\mathbf{w}_j - \mathbf{w}_k)^T \bar{\mathbf{q}} + \|\mathbf{w}_k\|^2 - \|\mathbf{w}_j\|^2$ .

With the upper bounds in (34) and (35), as well as any given local point  $\{\bar{\mathbf{q}}, \bar{\alpha}_{k,j}\}$ , problem (33) can be approximated as the following problem.

$$\min_{\zeta, \mathbf{q}, \boldsymbol{\alpha}} \quad \zeta + \rho_1 \bar{\phi} + \rho_2 \bar{\varphi} \quad (36a)$$

$$\text{s.t.} \quad (24f) - (24h), (29c), (30b) - (30c), \quad (36b)$$

where  $\bar{\varphi} = \sum_{k,j}^K (D_{k,j} - \theta_{k,j} + |\theta_{k,j}|)$ . Note that problem (36) is a convex optimization problem, which can be effectively solved by standard convex optimization tools such as CVX. It is worth noting that the feasible set of problem (36) is a subset of that of problem (33). Therefore, the objective value of problem (36) gives a lower bound to that of problem (33).

#### D. Overall Algorithm

The proposed iterative algorithm for problem (11)/(24) is concluded in Algorithm 3. Specifically, problem (24) is solved by optimizing  $f$  and subproblem (36) iteratively in an alternate manner. Since CVX invokes an interior-point method to solve the optimization problem, the

---

**Algorithm 3** Sub-optimal: Proposed Iterative Algorithm for Solving Problem (11).

---

- 1: Initialize the UAV location  $\bar{\mathbf{q}}$  and  $\bar{\boldsymbol{\alpha}}$ .
  - 2: **repeat**
  - 3:   Initialize  $l = 1$ ,  $\rho_1^0$  and  $\rho_2^0$ . Set  $b_1 > 1$ ,  $b_2 > 1$ ,  $\rho_1^{\max}$  and  $\rho_2^{\max}$ .
  - 4:   Update  $f$  based on (31) for given  $\bar{\boldsymbol{\alpha}}$ .
  - 5:   **repeat**
  - 6:     Solve problem (36) for given  $\{\bar{\mathbf{q}}, \bar{\boldsymbol{\alpha}}\}$ , and denote the optimal solution as  $\{\mathbf{q}^*, \boldsymbol{\alpha}^*\}$ .
  - 7:     Set  $\{\bar{\mathbf{q}}, \bar{\boldsymbol{\alpha}}\} \leftarrow \{\mathbf{q}^*, \boldsymbol{\alpha}^*\}$ .
  - 8:     Update  $l \leftarrow l + 1$ ,  $\rho_1^{l+1} \leftarrow \min\{b_1 \rho_1^l, \rho_1^{\max}\}$  and  $\rho_2^{l+1} \leftarrow \min\{b_2 \rho_2^l, \rho_2^{\max}\}$ .
  - 9:   **until** Convergence.
  - 10: **until** The fractional decrease of the objective value is below a threshold.
- 

computational complexity of the proposed algorithm is  $O(N_{ite}K^7)$ , where  $N_{ite}$  is the number of iterations for convergence in Algorithm 3.

*Remark 3:* In Algorithm 3, the initial UAV location  $\mathbf{q}^0$  and  $\boldsymbol{\alpha}^0$  should be carefully set. To this end, we propose a feasibility checking method for initial points. Specifically,  $\{\mathbf{q}^0, \boldsymbol{\alpha}^0\}$  is feasible to problem (24) only when the low-bound of  $p_k$  is no larger than its upper bound, i.e.,

$$\frac{\rho_0(2^{r^*} - 1)2^{r^*(K-f^0(k))}}{\sigma^2} (H^2 + \|\mathbf{q}^0 - \mathbf{w}_{f^0(k)}\|^2) \leq \tilde{P}_{f^0(k)}, \quad (37)$$

where  $f^0$  is obtained based on  $\boldsymbol{\alpha}^0$ .

## V. NUMERICAL RESULTS

In this section, numerical results are provided to evaluate the performance of the proposed algorithms. Unless being mentioned elsewhere, the reference SNR is set as  $\gamma_0 = 60$  dB. For IoT devices, the maximum transmit power is  $P_{\max} = 1$  W, circuit power consumption is  $P_c = 0.9$  W, and battery energy is  $E = 4 \times 10^3$  J. Moreover, the block error probability is set as  $\varepsilon_p^2 = 10^{-2}$ , the interference threshold is  $I_{th} = 28$  dBm, and the probability interference is  $\varrho = 0.1\%$ . In this network, we consider that  $K = 6$  IoT devices are randomly distributed in a horizontal plane, marked by ‘■’s.

In the following, the proposed optimal algorithm 2 (denoted as ‘Op-NOMA-J’) and sub-optimal algorithm 3 (denote as ‘Sub-NOMA-J’) are compared with two benchmark algorithms<sup>3</sup>:

<sup>3</sup>The optimal solution of the two benchmark algorithms can be obtained by using a similar method in Section II-B.

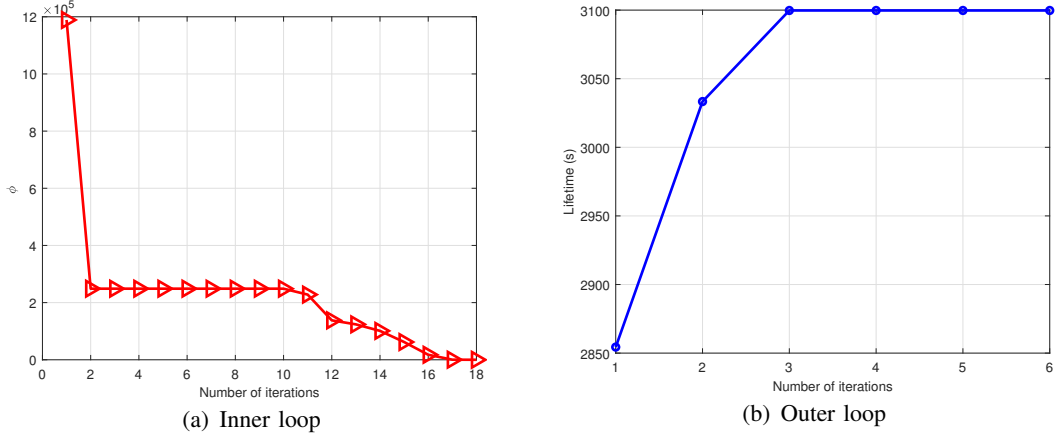


Fig. 2. Convergence performance of Algorithm 3.

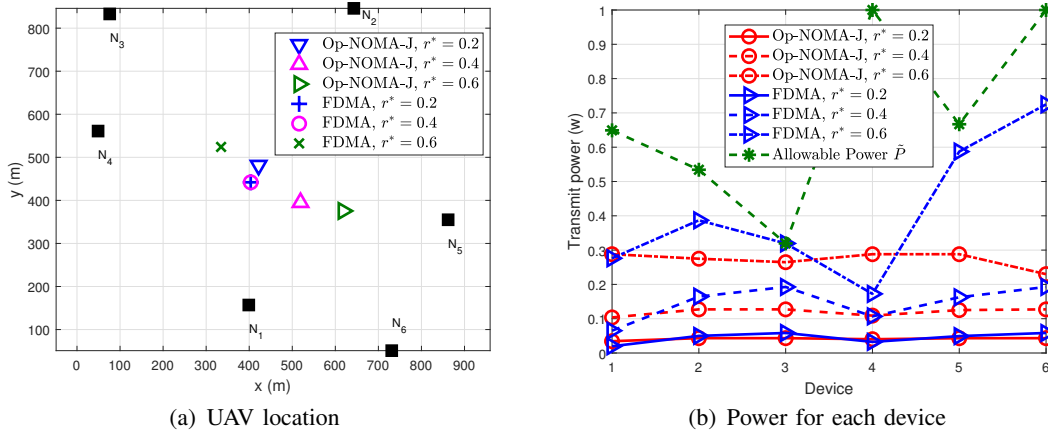


Fig. 3. Optimized UAV location and power under different  $r^*$  for Op-NOMA-J and FDMA.

- NOMA-P: For a UAV-enabled IoT network with cognitive NOMA transmission, the UAV location is fixed at the geometric center of IoT devices while the transmit power is optimized.
- FDMA: For a UAV-enabled IoT network with cognitive FDMA transmission [29], the UAV location and transmit power are jointly optimized.

In Fig. 2, we demonstrate the convergence performance of our proposed iterative algorithm 3 in terms of the outer-loop iteration and inner-loop iteration with  $r^* = 0.6$  bps/Hz. Fig. 2(a) shows the penalty value  $\varphi$  versus the number of iterations in the first inner loop. It can be observed that  $\varphi \rightarrow 0$  in the end. Fig. 2(b) shows the max-min lifetime versus the number of iterations in the outer loop. From the figure, the lifetime increases quickly with the number of iterations and the algorithm converges within 6 iterations.

Fig. 3 shows the UAV location and transmit power for Op-NOMA-J and FDMA under different

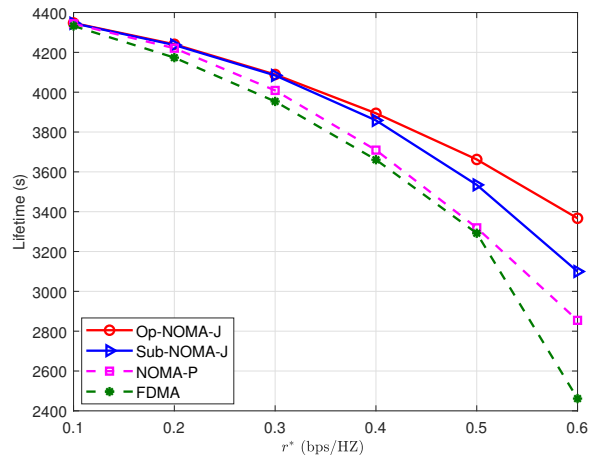


Fig. 4. Lifetime versus the QoS requirement  $r^*$  for different algorithms.

QoS requirements  $r^*$ . For FDMA, we observe from Fig. 3(a) that as  $r^*$  increases, the UAV flies toward device 3. This can be explained as follows. With the increase in  $r^*$ , each device rises its transmit power to satisfy the QoS requirement. Since the allowable transmit power of device 3, i.e.,  $\tilde{P}_3$ , is the bottleneck of the network (as shown in Fig. 3(b)), then once  $p_3^F$  approaches  $\tilde{P}_3$ , i.e.,  $p_3^F = \tilde{P}_3$ , the UAV can only move closer to device 3 to further improve the channel quality for the larger QoS requirement. On the contrary, for Op-NOMA-J, the UAV moves from the vicinity of the geometric center to away from device 3 and 4 as  $r^*$  increases. Note that the achievable rate of device 3 is given by  $R_3^N = \log_2(1 + \frac{p_3^N h_3^N}{I_0 + \sigma^2})$ , where  $I_0$  is the interference that device 3 has experienced,  $p_3^N$  is the transmit power and  $h_3^N$  is the channel gain. Owing to the small or even zero  $I_0$ , we can avoid reaching the upper bound of  $p_3^N$  too early when  $h_3^N$  reduces. Besides, this result reveals that with the growth of  $r^*$ , the distance discrepancy between the strongest and weakest devices to the UAV increases, or the discrepancy between the strongest and weakest channel gain increases. Moreover, from Fig. 3(b), when  $r^*$  is large, the transmit powers of all devices are quite distinct in Op-NOMA-J and FDMA, which is due to their different resource allocation mechanisms.

Fig. 4 shows the max-min lifetime versus the QoS requirement  $r^*$  for the different algorithms. It can be observed that the lifetime achieved by all the four algorithms rapidly decreases with the growth of  $r^*$ . This is expected since as  $r^*$  increases, all devices need to consume more transmit power to meet the QoS requirement, which degrades the lifetime performance. It can also be seen that the lifetime of the three NOMA-based algorithms significantly outperforms that of FDMA,

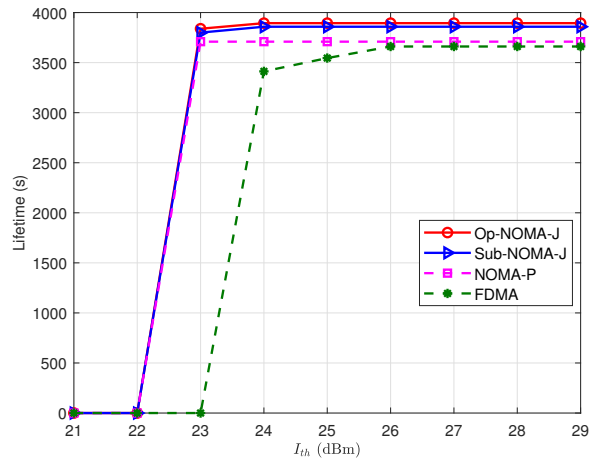


Fig. 5. Lifetime versus the interference threshold  $I_{th}$  for different algorithms.

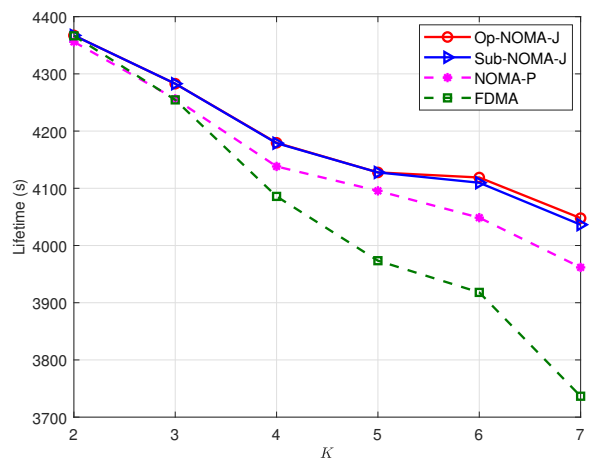


Fig. 6. Lifetime versus the device number  $K$  for different algorithms.

especially when  $r^*$  is large. This result indicates that NOMA is more effective than FDMA in improving the lifetime. Besides, the performance gap between NOMA-J (including Sub-NOMA-J and Op-NOMA-J) and NOMA-P becomes larger as  $r^*$  increases, which demonstrates the importance of the joint optimization of the UAV location, transmit power, and decoding order in enhancing lifetime performance.

Fig. 5 shows the max-min lifetime versus the interference threshold  $I_{th}$  for the different algorithms with  $r^* = 0.4$  bps/Hz. It can be observed that when  $I_{th}$  is very small (e.g.,  $I_{th} \leq 22$  dBm for the three NOMA-based algorithms and  $I_{th} \leq 23$  dBm for FDMA), the lifetime approaches zero. This is because there exists at least one IoT device whose transmit power cannot

satisfy strict probabilistic interference constraints. Furthermore, as  $I_{th}$  increases, the lifetime of all algorithms gradually increases before getting saturation at a sufficiently large  $I_{th}$ . The reason is that when  $I_{th}$  is moderate, the available transmit power increases with the relaxation of interference constraints, which provides higher flexibility in power control to achieve a better max-min lifetime. However, when  $I_{th}$  is sufficiently large, the interference constraints become loose while the power constraints are active by the QoS requirement and the maximum transmit power. Moreover, our proposed NOMA-J outperforms the other algorithms, which also validates the necessity of joint optimization of the UAV location, transmit power, and decoding order.

Fig. 6 shows the max-min lifetime versus the device number  $K$  for the different algorithms with  $r^* = 0.4$  bps/Hz. It can be observed that as  $K$  increases, the performance of FDMA sharply degrades while the three NOMA-based algorithms can maintain acceptable performance. In addition, the lifetime of FDMA is superior to that of NOMA-P when  $K = 2$ . However, with the growth of  $K$ , the performance of NOMA-P will surpass that of FDMA, and the lifetime gap between NOMA-P and FDMA becomes larger. From the figure, the proposed Op-NOMA-J always achieves the highest lifetime, especially when  $K$  is large, which further confirms the performance gain brought by NOMA. Moreover, the performance of Sub-NOMA-J is close to that of Op-NOMA-J when  $K \leq 5$ , and it can still reach more than 99.6% of the optimal performance when  $K = 7$ .

## VI. CONCLUSION

In this paper, we study the cognitive NOMA uplink transmission in UAV-enabled IoT networks. Specifically, the minimum lifetime of IoT devices is maximized via jointly optimizing the UAV location, transmit power, and decoding order without violating the QoS requirement and probability interference constraints with imperfect CSI. Although the formulated problem is non-convex, we solve it optimally via the Lagrange-duality-based algorithm, which entails high computational complexity. Furthermore, by equivalently transforming the original problem into a more tractable form, we propose a low-complexity iterative algorithm by leveraging the SCA technique and penalty method, which offers a sub-optimal solution. Moreover, we also unify two existing decoding order formulations. Numerical results demonstrate the effectiveness of joint UAV location, transmit power, and decoding order optimization. In practice, it is more preferable to use the Lagrange-duality-based algorithm in small-scale networks and to apply the iterative algorithm in large-scale networks. Moreover, future research could focus on extending

the problem to more practical scenarios, such as multi-UAV cooperative networks and massive MIMO UAV networks.

## APPENDIX A

### PROOF OF LEMMA 1

Define  $\beta_m \triangleq p_m h_m$ . According to (17), we have

$$\beta_m = (2^{r^*} - 1) \left( \sum_{n=m+1}^K \beta_n + \sigma^2 \right). \quad (38)$$

Hence,

$$\begin{aligned} \beta_m - (2^{r^*} - 1) \beta_{m+1} &= (2^{r^*} - 1) \left( \sum_{n=m+2}^K \beta_n + \sigma^2 \right) \\ &\stackrel{(a)}{=} \beta_{m+1}, \end{aligned} \quad (39)$$

where (a) is due to the definition of  $\beta_{m+1}$ . Then, we have

$$\beta_m = 2^{r^*} \beta_{m+1}. \quad (40)$$

Therefore,  $\{\beta_m\}_{m=1}^K$  forms a proportional sequence with a common ratio  $2^{-r^*}$ . By referring to the fact that  $\beta_K = (2^{r^*} - 1)\sigma^2$ , we have

$$\beta_m = (2^{r^*} - 1)\sigma^2 2^{(K-m)r^*}. \quad (41)$$

Consequently, we have

$$p_m = \frac{(2^{r^*} - 1)\sigma^2}{h_m} 2^{(K-m)r^*} = c_m (H^2 + \|\mathbf{q} - w_m\|^2), \forall m,$$

where  $c_m \triangleq \frac{(2^{r^*} - 1)\sigma^2}{\rho_0} 2^{(K-m)r^*}$ . ■

## APPENDIX B

### PROOF OF PROPOSITION 1

To prove proposition 1, we need the following Lemmas. We first define an intermediate variable  $X_k \triangleq \sum_{j=1}^K \alpha_{k,j}$ , whose property is given in Lemma 3.

*Lemma 3:* For any  $k \neq i$ , we have  $|X_k - X_i| \neq 0$ .

*Proof 7:* First, for  $\forall k \neq i$ , we have

$$\begin{aligned} X_k - X_i &= \sum_{j=1}^K \alpha_{k,j} - \sum_{j=1}^K \alpha_{i,j} \\ &= \alpha_{k,i} - \alpha_{i,k} + \sum_{j=1, j \neq k, i}^K (\alpha_{k,j} - \alpha_{i,j}), \end{aligned} \quad (42)$$

Due to constraints (24e) and (24g), we must have  $\alpha_{k,i} \neq \alpha_{i,k}$ . We will discuss the following two cases.

*a)*  $\alpha_{k,i} = 0, \alpha_{i,k} = 1$ : Referring to the fact that  $\alpha_{i,j} = 1 - \alpha_{j,i}$  and constraint (24h), we have

$$\alpha_{k,j} - \alpha_{i,j} = \alpha_{k,j} + \alpha_{j,i} - 1 \leq \alpha_{k,i} = 0 \quad (43)$$

Notice that in this case,  $\alpha_{k,i} - \alpha_{i,k} = -1$ , we have  $X_k - X_i \leq -1$ .

*b)*  $\alpha_{k,i} = 1, \alpha_{i,k} = 0$ : Since constraints (24h) holds for  $\forall k, i, j$ , by exchanging the index of  $i$  and  $j$  in (24h), we have

$$\alpha_{k,i} + \alpha_{i,j} - 1 \leq \alpha_{k,j}. \quad (44)$$

This leads to

$$\alpha_{k,j} - \alpha_{i,j} \geq \alpha_{k,i} - 1 = -\alpha_{i,k} = 0. \quad (45)$$

In this case,  $\alpha_{k,i} - \alpha_{i,k} = 1$  holds. Thus, we have  $X_k - X_i \geq 1$ .

Based on the above two cases, we conclude that

$$|X_k - X_i| \geq 1, \forall k \neq i, \quad (46)$$

which completes the proof. ■

*Lemma 4:* Define  $\alpha_{f(k), f(j)}^s = \alpha_{k,j}$  with  $f(k) \triangleq K - \sum_{j=1}^K \alpha_{k,j}$ . If  $\alpha$  satisfied constraints (24e)-(24h), then we have

$$\alpha_{f(k), f(j)}^s = \begin{cases} 1, & \forall f(k) < f(j), \\ 0, & \text{otherwise.} \end{cases} \quad \forall k, j. \quad (47)$$

*Proof 8:* Note that  $X_k \in \{0, 1, \dots, K-1\}$  since  $\alpha_{k,j} \in \{0, 1\}$ . By Lemma 3, we have  $|X_k - X_i| \neq 0, \forall k \neq i$ , then one can easily see that elements in  $\{X_k\}_{k=1}^K$  correspond to  $\{0, 1, \dots, K-1\}$  in a one-to-one manner. Therefore, by mapping  $k$  to  $f(k)$ , we can establish a new set  $\mathbf{X}^s \triangleq \{X_{f(k)}^s\}_{f(k)=1}^K$  with

$$X_{f(k)}^s = K - f(k). \quad (48)$$

Note that  $X_k = X_{f(k)}^s$ , we have  $X_k = X_{f(k)}^s = K - f(k)$ , which also determines the definition of  $f(k)$ , i.e.,  $f(k) = K - X_k = K - \sum_{j=1}^K \alpha_{k,j}$ .

Then, by letting  $\alpha_{f(k),f(j)}^s = \alpha_{k,j}$ , we can obtain a new sequence  $\alpha^s \triangleq \{\alpha_{f(k),f(j)}^s, k, j \in \mathcal{K}\}$ . In the following, we will give the closed-form expression of  $\alpha^s$ . Note that  $\alpha^s$  also meets constraints (24e)-(24h) and

$$X_{f(k)}^s = X_k = \sum_{j=1}^K \alpha_{k,j} = \sum_{j=1}^K \alpha_{f(k),f(j)}^s = \sum_{f(j)=1}^K \alpha_{f(k),f(j)}^s. \quad (49)$$

Combining (48) and (49), we obtain

$$\sum_{f(j)=1}^K \alpha_{f(k),f(j)}^s = K - f(k), \forall k. \quad (50)$$

Then, when  $f(k) = 1$ , we have  $\sum_{f(j) \neq 1}^K \alpha_{1,f(j)}^s = K - 1$  owing to  $\alpha_{1,1}^s = 0$ , which means

$$\alpha_{1,f(j)}^s = 1, \forall f(j) > 1. \quad (51)$$

Substituting (51) into constraints (24h), we have

$$\alpha_{f(j),1}^s = 0, \forall f(j) > 1. \quad (52)$$

Subsequently, when  $f(k) = 2$ , we have  $\sum_{f(j) \neq 2}^K \alpha_{2,f(j)}^s = K - 2$ . Owing to  $\alpha_{2,2}^s = 0$  and  $\alpha_{2,1}^s = 0$  from equation (52), we have

$$\alpha_{2,f(j)}^s = 1, \forall f(j) > 2. \quad (53)$$

Similarly, we have

$$\alpha_{f(j),2}^s = 0, \forall f(j) \geq 2. \quad (54)$$

By successively doing the same operations for  $f(k) \geq 3$ , we have

$$\alpha_{f(k),f(j)}^s = 1, \forall f(k) < f(j). \quad (55)$$

Substituting (55) into (24h), we obtain

$$\alpha_{f(k),f(j)}^s = \begin{cases} 1, & \text{if } f(k) < f(j), \\ 0, & \text{otherwise,} \end{cases} \quad \forall k, j, \quad (56)$$

which completes the proof. ■

Based on Lemma 3 and 4, we start to prove Proposition 1. Define  $p_{f(k)}^s = p_k$ ,  $h_{f(k)}^s = h_k$ ,  $\forall k$ . Constraints (24d) can be rewritten as

$$\begin{aligned}
r^* &\leq \log_2 \left( 1 + \frac{p_k h_k}{\sum_{j=1, j \neq k}^K \alpha_{k,j} p_j h_j + \sigma^2} \right) \\
&= \log_2 \left( 1 + \frac{p_k h_k}{\sum_{j=1, f(j) \neq f(k)}^K \alpha_{f(k), f(j)}^s p_{f(j)}^s h_{f(j)}^s + \sigma^2} \right) \\
&= \log_2 \left( 1 + \frac{p_k h_k}{\sum_{f(j)=f(k)+1}^K p_{f(j)}^s h_{f(j)}^s + \sigma^2} \right) \\
&= \log_2 \left( 1 + \frac{p_k h_k}{\sum_{f(j)=f(k)+1}^K p_j h_j + \sigma^2} \right). \tag{57}
\end{aligned}$$

■

## APPENDIX C

### PROOF OF PROPOSITION 2

We will show that  $\{\pi', \mathbf{p}'(\pi), \mathbf{q}\}$  is a feasible solution to problem (11) by proving that it meets constraints (8d), (10) and (11c). To this end, set  $\pi'(m) = f^{-1}(m) = k$  and  $\pi'(n) = f^{-1}(n) = j$ . Since  $\{\alpha, \mathbf{p}, \mathbf{q}\}$  is feasible to problem (24), we have

$$\begin{aligned}
r^* &\leq \log_2 \left( 1 + \frac{p_k h_k}{\sum_{f(j)=f(k)+1}^K p_j h_j + \sigma^2} \right) \\
&= \log_2 \left( 1 + \frac{p'_{\pi'(m)} h'_{\pi'(m)}}{\sum_{n=m+1}^K p'_{\pi'(n)} h'_{\pi'(n)} + \sigma^2} \right), \tag{58}
\end{aligned}$$

$$= \log_2 \left( 1 + \frac{p_k h_k}{\sum_{f(j)=f(k)+1}^K p_j h_j + \sigma^2} \right) \tag{59}$$

where we define  $h'_{\pi'(m)} = h_k$ . Thus,  $\{\pi', \mathbf{p}', \mathbf{q}\}$  meets constraints (8d).

Secondly, we will consider constraints (10). Define  $d_{f(k)}^s = d_k$ . Recall the fact that

$$\alpha_{k,j} = \begin{cases} 0, & \text{if } d_k > d_j, \\ 1, & \text{if } d_k < d_j, \\ 0 \text{ or } 1, & \text{if } d_k = d_j, \end{cases} \quad \forall k \neq j, \tag{60}$$

which indicates

$$(2\alpha_{k,j} - 1)(d_k - d_j) + |d_k - d_j| = 0. \tag{61}$$

Then, we obtain

$$(2\alpha_{f(k),f(j)}^s - 1)(d_{f(k)}^s - d_{f(j)}^s) + |d_{f(k)}^s - d_{f(j)}^s| = 0. \quad (62)$$

If  $f(k) < f(j)$ , we can find  $\alpha_{f(k),f(j)}^s = 1$  from Lemma 4, which leads to

$$d_{f(k)}^s - d_{f(j)}^s + |d_{f(k)}^s - d_{f(j)}^s| = 0, \forall f(k) < f(j), \quad (63)$$

or equivalently,

$$d_{f(k)}^s \leq d_{f(j)}^s, \forall f(k) < f(j). \quad (64)$$

In other words,

$$d_k \leq d_j, \forall f(k) < f(j). \quad (65)$$

Furthermore, referring to the fact that  $d'_{\pi'(m)} = d_k$  and  $d'_{\pi'(n)} = d_j$ , it follows

$$d'_{\pi'(m)} \leq d'_{\pi'(n)}, \forall m < n, \quad (66)$$

which indicates that  $\{\pi', \mathbf{p}', \mathbf{q}\}$  meets constraints (10).

Thirdly, it is obvious that  $\{\pi', \mathbf{p}', \mathbf{q}\}$  satisfies constraints (12c). In summary,  $\{\pi', \mathbf{p}', \mathbf{q}\}$  is a feasible solution to problem (11). Furthermore, define  $\bar{L}_1$  and  $\bar{L}_2$  as the objective value of problem (11) obtained at  $\{\pi', \mathbf{p}', \mathbf{q}\}$  and that of problem (24) obtained at  $\{\alpha, \mathbf{p}, \mathbf{q}\}$ . It is obvious that  $\bar{L}_1$  and  $\bar{L}_2$  only depend on  $\{p'_{\pi'(m)}, E_{\pi'(m)}\}$  and  $\{p_k, E_k\}$ , respectively. Since the same elements are arranged in different orders for  $\mathbf{p}$  and  $\mathbf{p}'$ , we have  $\bar{L}_1 = \bar{L}_2$ . ■

## APPENDIX D

### PROOF OF LEMMA 5

We will show that  $\{\tilde{\alpha}, \tilde{\mathbf{p}}, \mathbf{q}\}$  is a feasible solution of problem (24) by proving that it meets constraints (24c)-(24h). To see this, set  $\pi(m) = k$ ,  $\pi(n) = j$  and  $\pi(l) = i$ .

First, since  $\{\pi, \mathbf{p}, \mathbf{q}\}$  is feasible to problem (24d), we have

$$\begin{aligned} r^* &\leq \log_2 \left( 1 + \frac{p_{\pi(m)} h_{\pi(m)}}{\sum_{n=m+1}^K p_{\pi(n)} h_{\pi(n)} + \sigma^2} \right) \\ &= \log_2 \left( 1 + \frac{p_{\pi(m)} h_{\pi(m)}}{\sum_{m=1, m \neq n}^K \tilde{\alpha}_{\pi(m), \pi(n)} p_{\pi(n)} h_{\pi(n)} + \sigma^2} \right), \\ &= \log_2 \left( 1 + \frac{\tilde{p}_k \tilde{h}_k}{\sum_{j=1, j \neq k}^K \tilde{\alpha}_{k,j} p_j h_j + \sigma^2} \right), \end{aligned} \quad (67)$$

where we define  $\tilde{h}_k = h_{\pi(m)}$ . Thus,  $\{\tilde{\alpha}, \tilde{\mathbf{p}}, \mathbf{q}\}$  meets constraints (24d).

Secondly, we discuss constraints (24h) in the following four cases.

a)  $m < n < l$ : In this case, we have  $\tilde{\alpha}_{\pi(m),\pi(n)} = 1$ ,  $\tilde{\alpha}_{\pi(n),\pi(l)} = 1$  and  $\tilde{\alpha}_{\pi(m),\pi(l)} = 1$  such that  $\tilde{\alpha}_{\pi(m),\pi(n)} + \tilde{\alpha}_{\pi(n),\pi(l)} - 1 = \tilde{\alpha}_{\pi(m),\pi(l)}$ .

b)  $l < n < m$ : In this case, we obtain  $\tilde{\alpha}_{\pi(m),\pi(n)} = 0$ ,  $\tilde{\alpha}_{\pi(n),\pi(l)} = 0$  and  $\tilde{\alpha}_{\pi(m),\pi(l)} = 0$  and then  $\tilde{\alpha}_{\pi(m),\pi(n)} + \tilde{\alpha}_{\pi(n),\pi(l)} - 1 < \tilde{\alpha}_{\pi(m),\pi(l)}$ .

c)  $n < l, n < m$ : In this case, we have  $\tilde{\alpha}_{\pi(n),\pi(l)} = 0$  and  $\tilde{\alpha}_{\pi(m),\pi(l)} = 1$  such that  $\tilde{\alpha}_{\pi(m),\pi(n)} + \tilde{\alpha}_{\pi(n),\pi(l)} - 1 \leq \tilde{\alpha}_{\pi(m),\pi(l)}$  due to  $\tilde{\alpha}_{\pi(m),\pi(l)} \geq 0$ .

d)  $n > l, n > m$ : In this case, it has  $\tilde{\alpha}_{\pi(m),\pi(n)} = 1$  and  $\tilde{\alpha}_{\pi(n),\pi(l)} = 0$ . Hence,  $\tilde{\alpha}_{\pi(m),\pi(n)} + \tilde{\alpha}_{\pi(n),\pi(l)} - 1 \leq \tilde{\alpha}_{\pi(m),\pi(l)}$ .

Based on the above four cases, we conclude  $\{\tilde{\alpha}, \tilde{\mathbf{p}}, \mathbf{q}\}$  meets (24h).

Thirdly, we come to constraints (24e). Since  $\tilde{\alpha}$  always meets constraints (24e) when  $d_{\pi(m)} = d_{\pi(n)}$ , we only need to focus on when  $d_{\pi(m)} \neq d_{\pi(n)}$  in the following. Based on the definition of  $\tilde{\alpha}_{\pi(m),\pi(n)}$ , we have

$$\tilde{\alpha}_{\pi(m),\pi(n)} = \frac{1}{2} \left( \frac{|n-m|}{n-m} + 1 \right), \forall n \neq m. \quad (68)$$

Referring to the fact that  $d_{\pi(1)} \leq d_{\pi(2)} \leq \dots \leq d_{\pi(K)}$ , we have

$$\begin{cases} d_{\pi(m)} \leq d_{\pi(n)}, & \text{if } m < n, \\ d_{\pi(m)} \geq d_{\pi(n)}, & \text{if } m > n. \end{cases} \quad (69)$$

Thus, we have

$$\frac{|n-m|}{n-m} = \frac{|d_{\pi(n)} - d_{\pi(m)}|}{d_{\pi(n)} - d_{\pi(m)}}, \forall n, m \in \mathcal{M}_1, \quad (70)$$

where  $\mathcal{M}_1 \triangleq \{(n, m) \mid d_{\pi(m)} \neq d_{\pi(n)}, n \neq m\}$ . Substituting (70) into (68), we have

$$\tilde{\alpha}_{\pi(m),\pi(n)} = \frac{1}{2} \left( \frac{|d_{\pi(n)} - d_{\pi(m)}|}{d_{\pi(n)} - d_{\pi(m)}} + 1 \right), \forall n, m \in \mathcal{M}_1. \quad (71)$$

This indicates

$$\tilde{\alpha}_{\pi(m),\pi(n)} = \begin{cases} 0, & \text{if } d_{\pi(m)} > d_{\pi(n)}, \\ 1, & \text{if } d_{\pi(m)} < d_{\pi(n)}. \end{cases} \quad \forall n, m \in \mathcal{M}_1, \quad (72)$$

Hence,  $\{\tilde{\alpha}, \tilde{\mathbf{p}}, \mathbf{q}\}$  meets constraints (24e).

Finally, it is obvious that  $\{\tilde{\alpha}, \tilde{\mathbf{p}}, \mathbf{q}\}$  meets constraints (24c), (24f) and (24g). In summary,  $\{\tilde{\alpha}, \tilde{\mathbf{p}}, \mathbf{q}\}$  is a feasible solution to problem (24).

Furthermore, define  $\hat{L}_1$  and  $\hat{L}_2$  as the objective value of problem (11) obtained at  $\{\boldsymbol{\pi}, \mathbf{p}, \mathbf{q}\}$  and that of problem (24) obtained at  $\{\tilde{\alpha}, \tilde{\mathbf{p}}, \mathbf{q}\}$ . For the same reason in Appendix C, we have  $\hat{L}_1 = \hat{L}_2$ . ■

## REFERENCES

- [1] A. Zanella, N. Bui, A. Castellani, L. Vangelista, and M. Zorzi, "Internet of things for smart cities," *IEEE Internet Things J.*, vol. 1, no. 1, pp. 22–32, Feb. 2014.
- [2] M. Chen, Y. Ma, Y. Li, D. Wu, Y. Zhang, and C.-H. Youn, "Wearable 2.0: Enabling human-cloud integration in next generation healthcare systems," *IEEE Commun. Mag.*, vol. 55, no. 1, pp. 54–61, Jan. 2017.
- [3] X. Huang, T. Han, and N. Ansari, "On green-energy-powered cognitive radio networks," *IEEE Commun. Surveys Tuts.*, vol. 17, no. 2, pp. 827–842, 2nd Quart. 2015.
- [4] X. Xu, W. Yang, Y. Cai, and S. Jin, "On the secure spectral-energy efficiency tradeoff in random cognitive radio networks," *IEEE Jour. Sel. Areas Commun.*, vol. 34, no. 10, pp. 2706–2722, Oct. 2016.
- [5] O. Maraqa, A. S. Rajasekaran, S. Al-Ahmadi, H. Yanikomeroglu, and S. M. Sait, "A survey of rate-optimal power domain NOMA with enabling technologies of future wireless networks," *IEEE Commun. Surveys Tuts.*, vol. 22, no. 4, pp. 2192–2235, Sep. 2020.
- [6] L. Dai, B. Wang, Z. Ding, Z. Wang, S. Chen, and L. Hanzo, "A survey of non-orthogonal multiple access for 5G," *IEEE Commun. Surveys Tuts.*, vol. 20, no. 3, pp. 2294–2323, May 2018.
- [7] Q. Wu and R. Zhang, "Common throughput maximization in UAV-enabled OFDMA systems with delay consideration," *IEEE Trans. Commun.*, vol. 66, no. 12, pp. 6614–6627, Dec. 2018.
- [8] C. Zhan, Y. Zeng, and R. Zhang, "Energy-efficient data collection in UAV enabled wireless sensor network," *IEEE Wireless Commun. Lett.*, vol. 7, no. 3, pp. 328–331, Jun. 2017.
- [9] Y. Cai, Z. Wei, R. Li, D. W. K. Ng, and J. Yuan, "Joint trajectory and resource allocation design for energy-efficient secure UAV communication systems," *IEEE Trans. Commun.*, vol. 68, no. 7, pp. 4536–4553, Mar. 2020.
- [10] D.-H. Tran, V.-D. Nguyen, S. Chatzinotas, T. X. Vu, and B. Ottersten, "UAV relay-assisted emergency communications in IoT networks: Resource allocation and trajectory optimization," *IEEE Trans. Wireless Commun.*, pp. 1–1, 2021.
- [11] G. Zhang, X. Ou, M. Cui, Q. Wu, S. Ma, and W. Chen, "Cooperative UAV enabled relaying systems: Joint trajectory and transmit power optimization," *IEEE Trans. Green Commun. Netw.*, pp. 1–1, 2021.
- [12] H. Li and X. Zhao, "Throughput maximization with energy harvesting in UAV-assisted cognitive mobile relay networks," *IEEE Trans. Cogn. Commun. Netw.*, vol. 7, no. 1, pp. 197–209, Mar. 2021.
- [13] B. Ji, Y. Li, D. Cao, C. Li, S. Mumtaz, and D. Wang, "Secrecy performance analysis of UAV assisted relay transmission for cognitive network with energy harvesting," *IEEE Trans. Veh. Technol.*, vol. 69, no. 7, pp. 7404–7415, Jul. 2020.
- [14] P. X. Nguyen, V.-D. Nguyen, H. V. Nguyen, and O.-S. Shin, "UAV-assisted secure communications in terrestrial cognitive radio networks: Joint power control and 3D trajectory optimization," *IEEE Trans. Veh. Technol.*, vol. 70, no. 4, pp. 3298–3313, Apr. 2021.
- [15] Y. Huang, W. Mei, J. Xu, L. Qiu, and R. Zhang, "Cognitive UAV communication via joint maneuver and power control," *IEEE Trans. Wireless Commun.*, vol. 67, no. 11, pp. 7872–7888, Nov. 2019.
- [16] B. Liu, Y. Wan, F. Zhou, Q. Wu, and R. Q. Hu, "Robust trajectory and beamforming design for cognitive MISO UAV networks," *IEEE Wireless Commun. Lett.*, vol. 10, no. 2, pp. 396–400, Feb. 2021.
- [17] Z. Chu, W. Hao, P. Xiao, and J. Shi, "UAV assisted spectrum sharing ultra-reliable and low-latency communications," in *Proc. IEEE GLOBECOM*, 2019, pp. 1–6.
- [18] W. Chen, S. Zhao, R. Zhang, Y. Chen, and L. Yang, "UAV-assisted data collection with nonorthogonal multiple access," *IEEE Internet Things J.*, vol. 8, no. 1, pp. 501–511, Jan. 2021.
- [19] D. Zhai, H. Li, X. Tang, R. Zhang, Z. Ding, and F. R. Yu, "Height optimization and resource allocation for NOMA enhanced UAV-aided relay networks," *IEEE Trans. Commun.*, vol. 69, no. 2, pp. 962–975, Feb. 2021.

- [20] B. Hu, L. Wang, S. Chen, J. Cui, and L. Chen, "An uplink throughput optimization scheme for UAV-enabled urban emergency communications," *IEEE Internet Things J.*, pp. 1–1, 2021.
- [21] R. Zhang, X. Pang, J. Tang, Y. Chen, N. Zhao, and X. Wang, "Joint location and transmit power optimization for NOMA-UAV networks via updating decoding order," *IEEE Wireless Commun. Lett.*, vol. 10, no. 1, pp. 136–140, Jan. 2021.
- [22] D. Hu, Q. Zhang, Q. Li, and J. Qin, "Joint position, decoding order, and power allocation optimization in UAV-based NOMA downlink communications," *IEEE Syst. J.*, vol. 14, no. 2, pp. 2949–2960, Jun. 2020.
- [23] M.-J. Youssef, J. Farah, C. A. Nour, and C. Douillard, "Full-duplex and backhaul-constrained UAV-enabled networks using NOMA," *IEEE Trans. Veh. Technol.*, vol. 69, no. 9, pp. 9667–9681, Jun. 2020.
- [24] Y. Li, H. Zhang, K. Long, C. Jiang, and M. Guizani, "Joint resource allocation and trajectory optimization with QoS in UAV-based NOMA wireless networks," *IEEE Trans. Wireless Commun.*, pp. 1–1, 2021.
- [25] R. Tang, J. Cheng, and Z. Cao, "Joint placement design, admission control, and power allocation for NOMA-based UAV systems," *IEEE Wireless Commun. Lett.*, vol. 9, no. 3, pp. 385–388, Dec. 2020.
- [26] N. Tang, H. Tang, B. Li, and X. Yuan, "Cognitive NOMA for UAV-enabled secure communications: Joint 3D trajectory design and power allocation," *IEEE Access*, vol. 8, pp. 159 965–159 978, Sep. 2020.
- [27] N. Zhao, Y. Li, S. Zhang, Y. Chen, W. Lu, J. Wang, and X. Wang, "Security enhancement for NOMA-UAV networks," *IEEE Trans. Veh. Technol.*, vol. 69, no. 4, pp. 3994–4005, Feb. 2020.
- [28] W. Wang, J. Tang, N. Zhao, X. Liu, X. Y. Zhang, Y. Chen, and Y. Qian, "Joint precoding optimization for secure SWIPT in UAV-aided NOMA networks," *IEEE Trans. Commun.*, vol. 68, no. 8, pp. 5028–5040, Aug. 2020.
- [29] K. Chen, T. Chang, and T. Lee, "Lifetime maximization for uplink transmission in UAV-enabled wireless networks," in *Proc. IEEE WCNC*, Apr. 2019, pp. 1–6.
- [30] R. Ma, R. Wang, G. Liu, W. Meng, and X. Liu, "UAV-aided cooperative data collection scheme for ocean monitoring networks," *IEEE Internet Things J.*, vol. 8, no. 17, pp. 13 222–13 236, Mar. 2021.
- [31] J. Zhang, L. Zhu, Z. Xiao, X. Cao, D. O. Wu, and X.-G. Xia, "Optimal and sub-optimal uplink NOMA: Joint user grouping, decoding order, and power control," *IEEE Wireless Commun. Lett.*, vol. 9, no. 2, pp. 254–257, Feb. 2019.
- [32] J. Lu, Y. Wang, T. Liu, Z. Zhuang, X. Zhou, F. Shu, and Z. Han, "UAV-enabled uplink non-orthogonal multiple access system: Joint deployment and power control," *IEEE Trans. Veh. Technol.*, vol. 69, no. 9, pp. 10 090–10 102, June 2020.
- [33] F. Cui, Y. Cai, Z. Qin, M. Zhao, and G. Y. Li, "Multiple access for mobile-UAV enabled networks: Joint trajectory design and resource allocation," *IEEE Trans. Wireless Commun.*, vol. 67, no. 7, pp. 4980–4994, Apr. 2019.
- [34] Y. Xu, T. Zhang, D. Yang, Y. Liu, and M. Tao, "Joint resource and trajectory optimization for security in UAV-assisted MEC systems," *IEEE Trans. Commun.*, vol. 69, no. 1, pp. 573–588, Jan. 2021.
- [35] T. M. Nguyen, W. Ajib, and C. Assi, "A novel cooperative non-orthogonal multiple access (NOMA) in wireless backhaul two-tier hetnets," *IEEE Trans. Wireless Commun.*, vol. 17, no. 7, pp. 4873–4887, Jul. 2018.
- [36] H. Tang, Q. Wu, W. Chen, J. Wang, and B. Li, "Mitigating the doubly near-far effect in UAV-enabled WPCN," *IEEE Trans. Veh. Technol.*, vol. 70, no. 8, pp. 8349–8354, Jul. 2021.
- [37] M. S. Ali, H. Tabassum, and E. Hossain, "Dynamic user clustering and power allocation for uplink and downlink non-orthogonal multiple access (NOMA) systems," *IEEE Access*, vol. 4, pp. 6325–6343, Aug. 2016.
- [38] L. Musavian and S. Aissa, "Fundamental capacity limits of cognitive radio in fading environments with imperfect channel information," *IEEE Trans. Commun.*, vol. 57, no. 11, pp. 3472–3480, Nov. 2009.